Transactions of the 17th International Conference on Structural Mechanics in Reactor Technology (SMiRT 17)
Prague, Czech Republic, August 17 –22, 2003
Paper # G01-5

Updated Embrittlement Trend Curve for Reactor Pressure Vessel Steels

Mark Kirk[1)], Cayetano Santos[1)], Ernest Eason[2)], Joyce Wright[2)], G. Robert Odette[3)]

[1)] U.S. Nuclear Regulatory Commission, Washington DC, 20555
[2)] Modeling and Computing Services, Boulder, CO 80301
[3)] University of California at Santa Barbara, Santa Barbara, CA, 93106

ABSTRACT

The reactor pressure vessels of commercial nuclear power plants are subject to embrittlement due to exposure to high energy neutrons from the core. Irradiation embrittlement of RPV beltline materials is currently evaluated using US Regulatory Guide 1.99 Revision 2 (RG 1.99 Rev 2), which presents methods for estimating the Charpy transition temperature shift (ΔT_{30}) at 30 ft-lb (41 J) and the drop in Charpy upper shelf energy (ΔUSE). A more recent embrittlement model, based on a broader database and more recent research results, is presented in NUREG/CR-6551. The objective of this paper is to describe the most recent update to the embrittlement model in NUREG/CR-6551, based upon additional data and increased understanding of embrittlement mechanisms. The updated ΔT_{30} and USE models include fluence, copper, nickel, phosphorous content, and product form; the ΔT_{30} model also includes coolant temperature, irradiation time (or flux), and a long-time term. The models were developed using multi-variable surface-fitting techniques, understanding of the ΔT_{30} mechanisms, and engineering judgment. The updated ΔT_{30} model reduces scatter significantly relative to RG 1.99 Rev 2 on the currently available database for plates, forgings, and welds. This updated embrittlement trend curve will form the basis of revision 3 to Regulatory Guide 1.99.

KEYWORDS: embrittlement, embrittlement mechanisms, Charpy transition temperature shift model, reactor pressure vessel, Charpy upper shelf energy model

INTRODUCTION

In 1988 the NRC published Regulatory Guide 1.99 Revision 2 (RG 1.99 Rev 2) concerning the "Radiation Embrittlement of Reactor Vessel Materials." RG 1.99 Rev 2 sets forth procedures to estimate two measures of radiation embrittlement: the increase in the Charpy V-notch (CVN) transition temperature defined at 30 ft-lb (41 J) of absorbed energy (ΔT_{30}) and the reduction of the CVN energy on the upper shelf (ΔUSE) [1]. These measures are used in various ways throughout NRC regulations responsible for ensuring the integrity of the reactor pressure vessel under both routine operations and postulated accident scenarios [2][3].

Since the development of RG 1.99 Rev 2, continuing surveillance programs at U.S. power reactors have more than tripled the amount of available data on ΔT_{30} and ΔUSE. In addition, continuing research on radiation mechanisms and effects has produced a much deeper scientific understanding. The first major revisions of the RG 1.99 Rev 2 models were published in NUREG/CR-6551[4] in 1998, based on the larger database described below, as well as insight from mechanistic research on radiation effects. The transition temperature shift model in NUREG/CR-6551 was further modified and recalibrated to an expanded database in July 2000 to become the updated model presented here. The upper shelf energy model presented below is the same as in NUREG/CR-6551, reproduced here for completeness.

DATABASE

The database for the updated shift model begins with that reported previously in NUREG/CR-6551, which used the Power Reactor Embrittlement Database (PR-EDB) as its primary source [4][5]. The reported shifts and drops in the PR-EDB were determined using various techniques over many years, including visual inspection of raw Charpy plots and various statistical and graphical fitting techniques. To eliminate the inconsistencies and to ensure that repeatable, verifiable mean estimates of shift and drop were used, a computer program FITCV was written to fit all the raw Charpy data sets from the PR-EDB by least squares methods and to compute ΔT_{30} and ΔUSE directly from those fits. The general approach was to fit a modified hyperbolic tangent (*tanh*) curve to each set of raw Charpy data from the same heat of material tested at the same orientation and with the same neutron exposure. Then unirradiated and irradiated curves for the same heat and orientation were matched and transition temperature shifts and upper shelf energy drops with irradiation were computed.

Early in the project it was recognized that the fluences in the PR-EDB were inconsistently reported over a time span of nearly 30 years, during which time cross-section libraries and fluence evaluation methods changed substantially. Therefore, in response to an NRC staff request, the major domestic RPV manufacturers provided updated fluence values in early 1994.

The preliminary analysis database with updated fluences and consistently calculated ΔT_{30} and ΔUSE was provided to the ASTM E10.02.02 Task Group on Embrittlement Correlations for review and verification of entries for copper, nickel, phosphorous, fluence, material identification, weld wire heat numbers and weld flux types, and the Charpy properties. Corrected or updated values for some of these variables were provided by Task Group members, and they also provided and documented the coolant temperatures for the final NUREG/CR-6551 analysis database (cold leg temperatures for PWRs and recirculation temperatures for BWRs). Some additional surveillance data not yet in the PR-EDB were also provided and one shift was dropped from the database after review. All new or revised data were documented and entered into the database used for the final analysis. After the ASTM review, the modeling database for NUREG/CR-6551 was frozen for analysis in November 1996. There were 759 data records in the NUREG/CR-6551 database, but only 609 values of ΔT_{30} could be used at that time for model calibration, mainly because of incomplete information.

Soon after NUREG/CR-6551 was published, an effort began to expand the database in areas where it was sparse and to prepare an updated shift model. Many of the missing data were filled in, most commonly by determining previously-missing reactor coolant temperatures. Furthermore, 53 new records were added from surveillance capsules that had been tested and reported since the NUREG/CR-6551 database was frozen. The database for the updated model presented below was frozen in May of 2000 with a total of 740 complete records on pressure vessel steels, four of which were not used in fitting the updated shift model because they were extreme outliers according to the Chauvenet criterion (which was also used and described in [4]). This represented a net expansion of 21% in the database relative to that used in NUREG/CR-6551, roughly doubling the amount of data at long exposure times and increasing the number of weld data points by 25%.

PHYSICALLY ANTICIPATED TRENDS

Neutron irradiation of RPV steels causes embrittlement effects marked by an increase in yield strength that results from the fine scale microstructures produced by irradiation[6]. These microstructures obstruct dislocation motion, thereby increasing the stress required to move dislocations through these obstacles.[7][8] The mechanisms that produce these obstacles are (1) matrix hardening due to irradiation produced point defect clusters and dislocation loops, and (2) precipitation or age hardening due to irradiation-enhanced formation of copper-rich precipitates.[9] [10] A non-hardening form of embrittlement (i.e., one that elevates the toughness transition temperature without increasing the yield strength) occurs by grain boundary segregation of elements such as phosphorous. This embrittlement mechanism has never been observed in and is not expected for US RPV alloys; therefore, it is not discussed here.

Matrix Hardening

High energy neutrons interact with the atomic nuclei in reactor pressure vessel steels. The energy transferred during these interactions displaces iron atoms from their natural crystal lattice positions, producing microstructural defects such as vacancies and self interstitials. Increasing flux causes increased hardening due to these defects, but they occur relatively independently of alloy composition. The two types of matrix defects produced are unstable matrix defects (UMDs) and stable matrix defects (SMDs). UMDs are less than 1 nm in size and are composed of vacancy-solute clusters. They are produced directly from the initial displacement cascades but dissolve or annihilate quickly. Through diffusion the remaining defects and solutes in the microstructure evolve into lower energy configurations. The SMDs are complex vacancy solute clusters and nanovoids which do not fully dissolve at long times. The effect of these small microstructural features on hardening depends on the size, number, and volume fraction of these particles. The strength increase of a particular SMD feature is expected to vary with the square root of their number. Since the number of matrix features is proportional to fluence it is expected that the strength increase due to matrix hardening will also increase with the square root of fluence. At lower irradiation temperatures the annihilation of matrix defects by diffusion to grain boundaries or dislocations is reduced. Therefore, lower irradiation temperatures are expected to produce more matrix hardening.

Precipitation Hardening

Of the many alloying elements typical of RPV grade construction steels, copper is the primary element responsible for producing age hardening. Radiation enhances the diffusion and precipitation of supersaturated copper initially in solid solution, forming copper-rich precipitates (CRPs) that inhibit dislocation motion and, thereby, harden the material. This hardening increases the yield strength, producing a consequent increase in the fracture toughness transition temperature. This age hardening mechanism rises to a peak value and is then unaffected by subsequent irradiation, because no copper remains in solid solution to precipitate out and cause further damage. The magnitude of this peak depends on the amount of copper initially in solution and, therefore, available for subsequent precipitation. Post-weld heat treatment (PWHT) performed before the RPV is placed into service can also precipitate copper, thereby removing some of it from solid solution and eliminating its ability to cause further damage during irradiation. Thus, different materials and product forms may exhibit different peak hardening values due to differing pre-service thermal treatments. Additionally, the presence of nickel in the alloy further enhances its precipitation hardening capacity.

Nickel and manganese precipitate along with copper, forming larger second-phase particles that present greater impediments to dislocation motion and, thereby, produce a greater hardening effect.

Irrespective of the bulk amount of copper in the alloy, only a limited amount of copper can be held in solid solution in the ferrite matrix. Most of the bulk copper above this limit precipitates from the ferrite matrix at the final heat treatment temperature and, therefore, is not available for subsequent precipitation during irradiation. The solubility limit of copper in ferrite at the final heat treat temperature establishes this limit, thereby establishing the maximum amount of copper that can form into CRPs during subsequent irradiation. Based on typical post-weld heat treatment (PWHT) temperatures, estimates of the maximum amount of copper which can remain in solution is about 0.3 wt% [11][12]. However, in order for a steel to experience any hardening by this mechanism, the bulk copper must *exceed* the solubility limit of copper at the reactor operating temperature (approximately 280°C or 550°F). At this temperature the solubility limit of copper decreases to < .1 wt%.

Given adequate time at reactor operating temperatures (i.e. times greatly exceeding the duration of currently operational licenses) precipitation of copper can occur under the influence of temperature alone, providing a classical age hardening mechanism. However, in RPV materials irradiation produces vacancies in the microstructural lattice, which enhances the diffusion and precipitation of CRPs from the ferrite matrix. As mentioned previously, copper precipitation continues as long as irradiation continues until copper has been depleted from the matrix. At this point no excess copper remains in the matrix to be precipitated out, and the process naturally stops. A minimum amount of copper in the range of 0.05 to 0.1 wt% is needed in order to nucleate these precipitates.

While copper is the element primarily responsible for age hardening in RPV steels, other elements such as nickel, manganese, phosphorous, and silicon can also precipitate along with copper [13] [14]. Manganese and nickel are prime candidates for the formation of copper-alloyed precipitates, because they are the primary alloying elements used in RPV steels (i.e. they are present in the greatest weight percent). These copper-alloyed precipitates produce still larger impediments to dislocation motion, thereby further hardening the material. The amount of such alloying elements depends in part on product form, hence the amount of age hardening is expected to vary with product form.

Vacancy concentrations, hence solute diffusion and precipitation rates, increase with both increasing temperatures and neutron flux or dose rate. Depending on the irradiation/temperature conditions present, both thermally driven and irradiation driven precipitation can be active at the same time. However, radiation enhanced diffusion tends to dominate over thermal diffusion for most typical PWR dose rates at ≈280°C (550°F). In contrast, dose rates are much lower in boiling water reactors. In this case thermal diffusion may contribute to copper precipitation at long times. Thus fluence (ϕt) alone might not be the only exposure variable needed in the precipitation hardening term, which would also depend on variables such as time (t) or flux (ϕ), which controls the time needed to reach a specified ϕt. Thermal contributions to diffusion and precipitation hardening are only one of several mechanisms that lead to flux, or time at temperature, effects. It is also noted that these effects operate in the pre-plateau region for precipitation hardening. Thus dose rate effects are not expected to influence either the ultimate level of precipitation hardening due to copper or the matrix feature contribution[15][16][17][18][19].

UPDATED TRANSITION TEMPERATURE SHIFT MODEL

The starting point for calibration of the updated transition temperature shift model developed for inclusion in Revision 3 of Regulatory Guide 1.99 is the transition temperature shift model reported previously as Eq. 4-1in NURUG/CR-6551. While the NUREG/CR-6551 model fits the 1996 database reasonably well, several factors were not well modeled in the expanded database and therefore received particular attention in the 2000 update:

- After long exposure times, ΔT_{30} appears to be significantly under predicted by the NUREG/CR-6551 model. Since RPV service exposure times greatly exceed the exposure times of surveillance capsules, unconservative predictions at long times are a serious concern, and a key objective of the model update was to collect all available long-time data and develop a method to address this "long time bias." The bias was noticeable in the original NUREG/CR-6551 database and was partially reflected in the exponent on fluence in the matrix damage term of the NUREG/CR-6551 model, which increased as a function of fluence. But as the number of long time points doubled in the updated database, the effect became clearly different from fluence and significant statistically. This long-time effect was also partly confounded with the flux/time term in the NUREG/CR-6551 model, so a means was devised for blocking the partial confounding with fluence effects and separately calibrating the two time-related effects.

- In addition it was discovered that for the subset of data on plate materials (A533 and A302), shifts for plates in vessels manufactured by Combustion Engineering (CE) tended to be under predicted, while shifts for plates in vessels from other manufacturers tended to be over predicted. While a physical explanation for this observation has not yet been developed, this "vessel manufacturer effect" was found to be highly statistically significant.

- Another effect investigated was the lower apparent saturation level of copper for welds fabricated with Linde 80 and 0091 flux when compared to welds fabricated using other weld fluxes. In the expanded database, there were 25% more weld observations, which made it feasible to refine the copper model by defining two distinct copper saturation levels for different weld classes. Based on the information now available on embrittlement mechanisms, this effect is thought to relate to the nickel content of the weld and post-weld heat treatment, among other factors, rather than flux per se. The flux categories are merely used to divide the welds into groups that appear to have similar saturation levels in the available data.

Calibration Approach For Updated Shift Model

The analysis methodology described for the shift model in NUREG/CR-6551 was generally followed in the updating effort. One difference is that the NUREG/CR-6551 model was calibrated all at once, to all the data. In the update, a few of the fitting constants were determined from runs on a relevant subset of the data, so that the most relevant data would be used to calibrate each part of the model, as described below. These constants were then held fixed while the rest of the fitting constants were calibrated. The result of this sequential calibration approach is less possibility of confounding between effects.

Both exposure time and fluence appear twice in the updated model, which could potentially cause numerical trade-offs between terms and instability of the fitted fluence and time model constants. Moreover, time and fluence are physically related, so the fitting process was designed to ensure that the fluence residuals are flat (no unmodeled residual effect of fluence) while investigating the time and/or flux-related effects. The fluence terms in the matrix hardening and age hardening terms did not numerically trade off with each other, and similar results for the matrix hardening fluence exponent were obtained on both the whole dataset and the low copper data (where the age hardening term is zero). To minimize possible numerical trade-offs between the flux-time term and the long-time bias term, the flux-time parameter was calibrated only to the subset of data with exposure times shorter than 97,000 hr (688 points). The long time bias was calibrated by determining the average of the increased shifts at long time (>97,000 hr), calculated heat by heat, for only those heats that had both short and long time shift data available (48 long-time shifts, 144 short-time shifts in 33 heats). This heat-by-heat analysis process eliminated the possibility of confounding from unmodeled heat effects, and as noted above, the residuals with fluence were flat so that no confounding of fluence and long-time effects would occur. Only five of the 48 long-time points were at low enough flux for the flux-time term to be relevant, and none of the short-time data were relevant to the long-time term by definition; thus, this approach ensured that the most relevant data were used to calibrate each time term, reasonably clear of confounding from other terms.

The coolant temperature activation energy in the matrix hardening term was not well determined by the full data set. Some preliminary fits indicated a possibly different temperature effect in the long-time points (>97,000 hr.), so trade-offs between different temperature effects in the long-time and short-time data might have caused the difficulties. There were no numerical instability problems when the temperature parameter was fitted to the set of 688 short-time points, so it was calibrated to the short time data set, then the possibility of a different long-time temperature effect was investigated using residual analysis. A different temperature slope is apparent in the long-time residuals, consistent with a possible thermal explanation for the long-time effect, but the slope of the temperature residuals is not large enough on 48 points to be significantly different from zero. Hence a different temperature effect at long time was not included in the updated model, though this issue should be revisited when additional long-time data are available.

The 97,000 hr. breakpoint between short- and long-time points was determined from numerous calibration runs with a tanh function, which allows the transition location (breakpoint) to be directly determined by the data. In these runs, the hyperbolic tangent form degraded to essentially a step function, with a constant increase in shift for exposure times exceeding 97,000 hr. A few other smooth functions in addition to the tanh function were tried to represent the transition from short to long time behavior, but the lack of data near the breakpoint caused the same quality of fit to be obtained with many different functions. Consequently, the simplest possible function, a constant bias above the breakpoint, was set equal to the average of the heat-by-heat increases in shift, and the breakpoint time and average bias were held fixed during calibration of the rest of the model parameters. Since practical applications of the embrittlement model are at times well above the 97,000 hr. breakpoint, the precise value of that time and the functional shape near that time are not of great practical interest.

Updated Shift Model

The updated fit, recommended for Revision 3 of Regulatory Guide 1.99, is as follows:

(Eq 1)

$$\Delta T_{30} = A\exp\left(\frac{19310}{T_c + 460}\right)\left(1 + 110P\right)\left(\phi t\right)^{0.4601} + B\left(1 + 2.40Ni^{1.250}\right)f\left(Cu\right)g\left(\phi t\right) + Bias$$

$$A = \begin{Bmatrix} 8.86\text{x}10^{-17}, \text{welds} \\ 9.30\text{x}10^{-17}, \text{forgings} \\ 12.7\text{x}10^{-17}, \text{plates} \end{Bmatrix} \qquad B = \begin{Bmatrix} 230, \text{welds} \\ 132, \text{forgings} \\ 206, \text{plates in CE fabricated vessels} \\ 156, \text{all other plates} \end{Bmatrix}$$

$$f\left(Cu\right) = \begin{Bmatrix} 0, Cu \le 0.072 \text{ wt\%} \\ \left(\text{Cu} - 0.072\right)^{0.659}, Cu > 0.072 \text{ wt\%} \end{Bmatrix} \qquad g\left(\phi t\right) = \frac{1}{2} + \frac{1}{2}\tanh\left[\frac{\log\left(\phi t + 4.579\text{x}10^{12}\, t_i\right) - 18.265}{0.713}\right]$$

$$Cu_{\max} = \begin{Bmatrix} 0.25, \text{for welds with Linde 80 or Linde 0091 flux} \\ 0.305, \text{for everything else} \end{Bmatrix} \qquad Bias = \begin{Bmatrix} 0, t_i < 97000 \text{ h} \\ 9.4, t_i \ge 97000 \text{ h} \end{Bmatrix}$$

Here, all temperatures are in °F, *Cu*, *Ni*, and *P* are in wt%, times are in hours, and ϕt is in n/cm^2.

Table 1 summarizes standard deviations for specific data subsets and the overall standard error of all 736 calibration data points about Eq 1, which is 21.5°F (11.9°C). This is an overall improvement compared to the standard error of the NUREG/CR-6551 model, which was 23.0°F (12.8°C), and the RG 1.99 Rev 2 model, where the standard deviation is 26.6°F (14.8°C) (in both cases on the 609 points used in NUREG/CR-6551). The greatest reductions in scatter are in the shift predictions for plates and welds. There is a statistically significant difference between the standard deviations in Table 1 for all welds pooled together *vs*. those for all base metals pooled together (i.e., both plate categories plus forgings). However, there is no statistically significant difference in the standard deviations between the two weld types, or between the three base metal types.

Data subset	Number of points	S_d about Eq. 1, °F (°C)
Forgings	118	19.3 (10.7)
Plates, CE vessels	182	21.0 (11.7)
Plates, non-CE vessels	204	19.5 (10.8)
Welds, Linde 80 or Linde 0091 flux	97	24.0 (13.3)
Welds, Linde 1092 or other flux	135	23.6 (13.1)
All base metals	504	20.0 (11.1)
All welds	232	23.8 (13.2)
All Materials	736	S_e = 21.5 (11.9)

Table 1 Standard Deviations for subsets of data**.**

The goodness of fit of Equation 1 to the calibration data is shown graphically in Figure 1, which compares the predicted versus actual shift, with dashed lines that enclose 90% of the calibration data.

Discussion of Updated Shift Model

Equation 1 includes the following physically anticipated features:

- two main damage terms, corresponding to matrix hardening and age hardening,
- a (nearly) square root dependence on fluence in the matrix hardening term,
- an effect of temperature on matrix hardening,
- an effect of phosphorus on overall shift (this effect is not specifically a matrix hardening effect; it is included in the matrix hardening term but can be algebraically separated out),
- a product form dependency reflecting known differences in manganese, microstructure, thermal treatment, and other manufacturing-related factors
- an age hardening term that includes
    - a threshold copper level below which no age hardening occurs and a maximum effective copper level that appears to depend on Ni, post weld heat treatment, and other factors,
    - a saturation in age hardening with fluence at high copper levels,
    - synergistic effects of copper, nickel, and fluence.

In addition, this model also includes a number of features that are empirically derived, some of which also have an emerging physical understanding, including:

- a synergistic effect of flux and/or time in addition to fluence in the age hardening term,
- an effect of vessel manufacturer on the plate behavior,
- an additional damage effect, beyond that of the two main terms, that only becomes apparent at long time.

Thus, while the overall form of Equation 1 is broadly consistent with a physical understanding of irradiation damage mechanics, certain terms in Equation 1 rely more heavily on an empirical understanding of irradiation effects to support their inclusion and the specific forms used to calibrate them. Effects were included in the model for strong physical reasons, for strong statistical reasons, and/or to avoid unconservative predictions in practical applications.

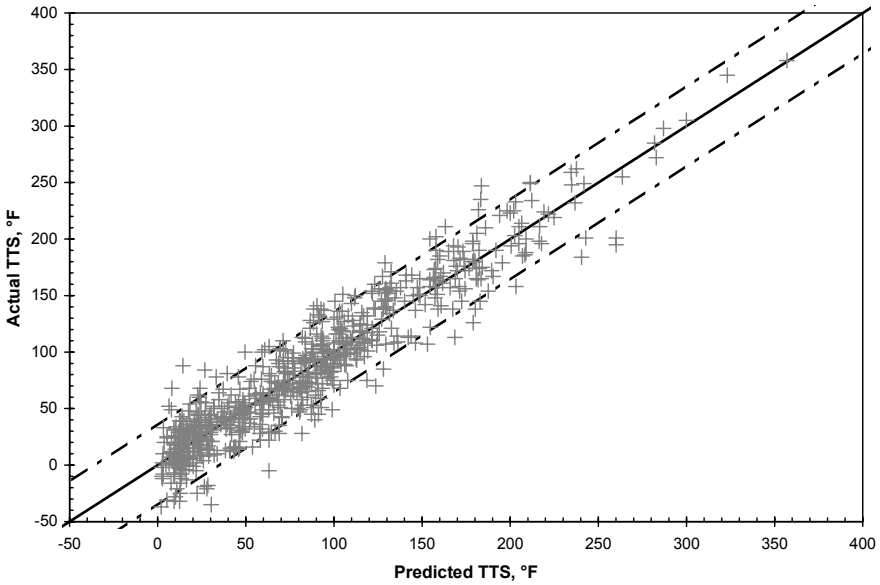

Fig. 1 Predicted versus measured 30 ft-lb (41J) transition temperature shifts.

The inclusion of statistically-justified empirical effects and terms that avoid unconservative predictions under certain circumstances, despite a lack of complete physical understanding in some cases, is deliberate and consistent with RG 1.99 Rev 1 and 2 and most other regulatory guides and engineering codes. All of the empirical effects are statistically significant over the relevant subset of data at the 95% level or higher except the use of different product form constants in the "A" coefficient on the matrix damage term. That feature is retained, even though not significant for all the low-copper data affected by it, to avoid potentially unconservative predictions for plates with low copper. Other effects are statistically significant on particular subsets of data but would not be a significant effect over the entire database. An example is the flux-time effect, which is highly significant statistically on the low-flux, typical BWR data, but almost completely irrelevant to the other 93% of the database at higher flux, where any such effect is (and would be expected to be) small. It is included both because of the statistical significance and to avoid unconservative predictions for low-flux conditions; in addition there is an emerging physical basis for it. Another example is the long time bias term, which is significant on the 33 heats which have both short and long time data and for predicting the 48 data points with more than 97000 hr exposure, but the effect appears to be completely absent in the 688 points at shorter time. This effect is required to avoid unconservative predictions under the conditions where the model most often will be used – at long operating times. A final example is the "vessel manufacturer" effect in the "B" coefficient of Eq. 1, which is highly significant in the plate data where it was discovered empirically. So far there is no accepted physical reason for the effect, but knowing that it is highly significant statistically is the first step toward eventually determining the cause.

UPPER SHELF ENERGY MODEL

Little guidance was available from embrittlement mechanism research to help with formulation of the upper shelf model. For this reason the procedure used in NUREG/CR-6551 and briefly described in this section to estimate ΔUSE is mainly empirical, as described in more detail in NUREG/CR-6551. The overall approach used a combination of numerical transformation analysis, least squares fitting of candidate models, and analysis of residuals, similar to that used in several previous projects that characterized materials behavior[20][21]. The quality of each candidate model was assessed by evaluating the standard error of estimate of the measured data about the model prediction, reviewing plots of each of the independent variables versus the dependent variable (normalized relative to the variables not shown), analyzing residual plots for all independent variables, and comparing measured versus predicted values of the dependent variable, which was the irradiated upper shelf energy, USE_i.

Several independent variables and some combinations of variables were found to be effective for modeling USE_i, including USE_u (the strongest individual predictor variable), fluence, Cu, and a combination of Cu, Ni, and fluence. Irradiation temperature was not found to be an important variable. There was some indication that the effects of Cu and fluence saturate for Cu greater than about 0.3 wt%, which was consistent with the preliminary work on the ΔT_{30} model.

The best correlation found for predicting USE_i was:

$$USE_i = A + 0.0570 \cdot USE_u^{1.456} - \left[17.5 \cdot f(Cu) \cdot \left(1 + 1.17 Ni^{0.8894}\right) + 305P\right]\left(\frac{\phi t}{10^{19}}\right)^{0.2223} \quad \text{(Eq.2)}$$

A = 55.4 for welds
61.0 for plates
66.3 for forgings

$$f(Cu) = \frac{1}{2} + \frac{1}{2}\tanh\left[\frac{Cu - 0.138}{0.0846}\right]$$

Here, all upper shelf energies are in ft-lb, *Cu*, *Ni*, and *P* are in wt%, and ϕt is in n/cm^2.

The goodness of fit of Eq 2 is demonstrated graphically in Figure 2, which shows the predicted USE_i versus the actual USE_i with bounds that enclose 90% of the data. The quality of fit of the calibration data about the model is excellent. The standard error of 11.2 ft-lb (15J) is not much greater than the experimental error one would expect in repeated USE tests of the same material at various laboratories.

Note that Equation 2 allows negative drops (increases) in upper shelf energy with irradiation, which did appear frequently in the database (113 observations). It is not clear what physical effect, if any, would cause USE to increase with irradiation; one hypothesis is measurement error in the original USE_u value.

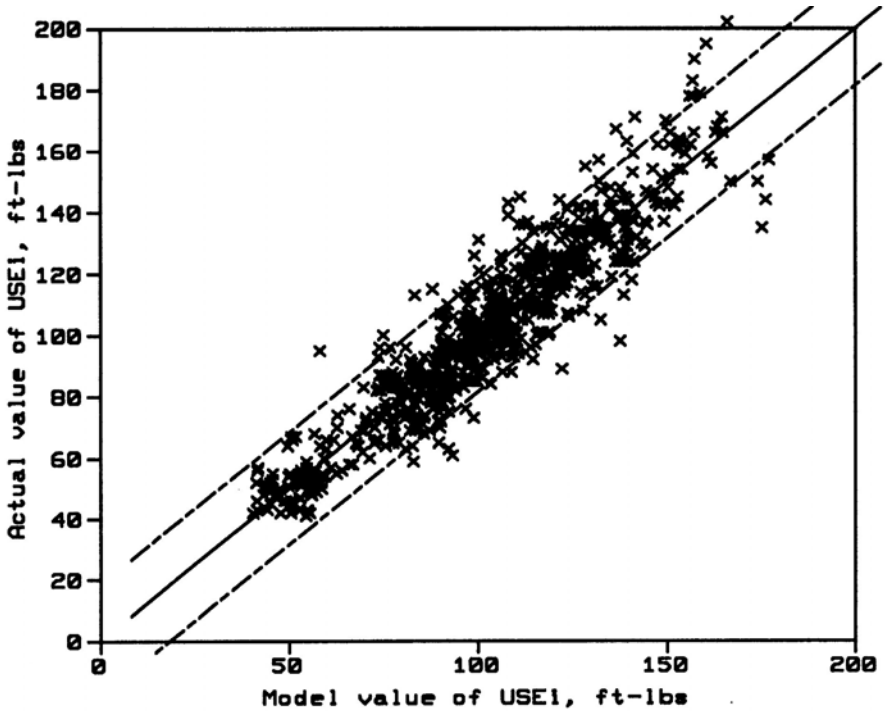

Fig. 2. Predicted versus measured irradiated upper-shelf energies.

CONCLUSIONS

Since the publication of RG 1.99 Rev 2 in 1988, the amount of surveillance data and the physical understanding of the mechanisms responsible for irradiation damage in reactor pressure vessel steels have both increased considerably. This information was used to improve models for estimating increases in CVN transition temperatures and drops in CVN upper shelf energy due to irradiation. The new models are greatly improved relative to those in RG 1.99 Rev 2, with standard deviations of 21.5 F (12°C)and 11.2 ft-lb (15J) for the transition temperature shift and upper shelf energy models respectively. The updated shift model is also improved relative to the one previously published in NUREG/CR-6551, again by the use of additional data and physical insights. These new models will be used for revision 3 to Regulatory Guide 1.99.

REFERENCES

1 U.S Nuclear Regulatory Commission, Regulatory Guide 1.99 Revision 2, "Radiation Embrittlement of Reactor Vessel Materials," May 1988.

2 Code of Federal Regulation 10CFR50.61, "Fracture Toughness Requirements for Protection Against Pressurized Thermal Shock Events."

3 Code of Federal Regulation 10CFR50 Appendix G, "Fracture Toughness Requirements {for Normal Operation}."

4 Eason, E.D., J.E., Wright, and G.R. Odette, "Improved Embrittlement Correlations for Reactor Pressure Vessel Steels," NUREG/CR-6551, U.S. Nuclear Regulatory Commission, Washington DC 1998.

5 Stallman, F.W., F.B.K. Kam, and B.J. Taylor, "PR-EDB: Power Reactor Embrittlement Database," NUREG/CR-4816, U.S. Nuclear Regulatory commission, Washington DC 1990.

6 Odette, G.R., P.M. Lombrozo, R.A. Wullaert, "The Relationship Between Irradiation Hardening and Embrittlement of Pressure Vessel Steels," ASTM STP 870, American Society of Testing and Materials, Philadelphia, PA, 1985, pp. 840-860.

7 Odette, G.R., "On the Dominant Mechanism of Irradiation Embrittlement in Pressure Vessel Steels," Scripta Met., 11, 1983, p.1183.

8 Odette., G.R., G.E. Lucas, "Recent Progress in Understanding Reactor Pressure Vessel Steel Embrittlement," Radiation Effects and Defects in Solids, 144, 1998, pp.189-231.

9 Odette, G.R., and B.D. Wirth, "A Computational Microscopy Study of Nanostructural Evolution in Irradiated Pressure Vessel Steels, J. Nucl. Mater., 251, 1997, pp. 157-171.

10 Fisher, S.B., and J.T. Buswell, "A Model for PWR Pressure Vessel Embrittlement," Int. Journal of Pressure Vessels and Piping, 27-2, 1987, pp.91-135.

11 Odette, G.R., and G.E. Lucas "Recent Advanced in Predicting Embrittlement of Reactor Pressure Vessel Steels," Proceedings of the 2nd International Symposium on Environmental Degradation in Nuclear Reactors-Water Reactors, J.T.A. Roberts, J.R. Weeks, G.J Theus, eds., American Nuclear Society, La Grange Park, IL, 1986, p.345.

12 Odette, G.R. and G.E. Lucas "The Effect of Heat Treatment on Irradiation Hardening of Pressure Vessel Steels," Proceedings of the 3rd International Symposium on Environmental Degradation in Nuclear Reactors-Water Reactors, J.R. Weeks, G.J Theus, eds., The Metallurgical Society, Warrendale, PA, 1988, p.95.

13 Mader, E., "Kinetics of Irradiation Embrittlement and the Post-Irradiation Annealing of Nuclear Reactor Pressure Vessel Steels, PhD. Thesis, UC Santa Barbara, 1995.

14 Liu, C.L., G.R. Odette, B.D. Wirth, G.E. Lucas, "A Lattice Monte Carlo Simulation of Nanophase Compositions and Structures in Irradiated Pressure Vessel Fe-Cu-Ni-Mn-Si Steels," Matls Sci and Eng., A238, 1997, pp.202-209.

15 Odette, G.R., G. E. Lucas and D. Klingensmith, "Anomalous Hardening in Model Alloys and Steels Thermally Aged at 290^{O}C and 350^{O}C: Implications to Low Flux Irradiation Embrittlement", Effects of Radiation on Materials-18 ASTM-STP-1325 (1999) 1089.

16 Odette,G.R., and C. Cowan, "Use of Combined Electrical Resistivity and Seebeck Coefficient Measurements to Characterize Solute Redistribution Under Irradiation and Thermal Aging," Proceedings of the 10th International Symposium on Environmental Degradation of Materials in Light Water Reactors, NACE (2001)

17 Odette, G.R., G.E. Lucas and D. Klingensmith, "On the Effect of Neutron Flux and Composition on Hardening of Reactor Pressure Vessel Steels and Model Alloys", Microstructure in Irradiated Materials-2000, MRS Symp. Proc. 650 (2001) R6.9.

18 Williams, T.J., D. Ellis, C. A. English and J. Hyde, " A Model of Irradiation Damage in High Nickel Submerged Arc Welds", Int. Jour. of Pressure Vessels and Piping, 79 (2002) 64.

19 Workshop on Dose Rate Effects in Reactor Pressure Vessel Materials Held November 12-14, 2001, Olympic Valley CA, Electric Power Research Institute Conference Proceedings (CD), EPRI 1006981 (2002).

20 Eason, E.D. and E.E. Nelson, "Improved Model for Predicting J-R Curves from Charpy Data," NUREG/CR-5356, Washington DC, 1989.

21 Eason, E.D., J. Wright, and E.E. Nelson,"Multivariable Modeling of Pressure Vessel and Piping J-R Data," NUREG/CR-5729, Washington DC 1991.